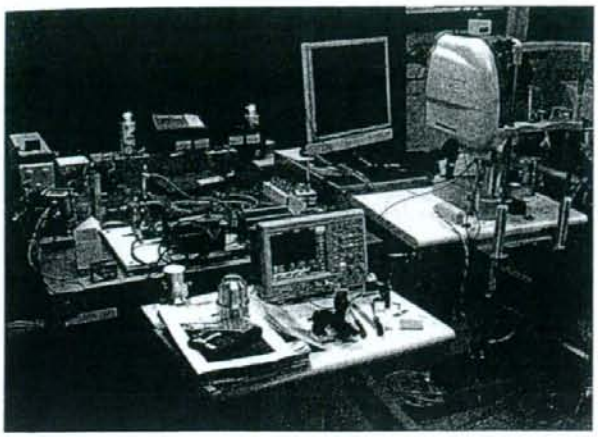

図5　東京医療センター，理化学研究所，(株)ニデックで共同開発中の functional OCT 試作器
Functional OCT と網膜内因性信号をともに記録することができる。

ズレが致命的になるのである。これは高解像度で functional imaging を行う場合に共通の問題点であるが，OCT は微細な構造を捉えているために特にその影響を受けやすい。解決策として，各画像間でピクセル値の相関を計算して位置合わせ（re-arrangement）を行うことや，OCT のスキャンスピードを速くすることなどが挙げられる。

次に，信号の発生起源が不明瞭な点である。動物種の違いがあるとはいえ，上述の 2 施設の実験結果を比べてみても，その信号の性質にはあまりの開きがある。特に，最近はさまざまな研究施設が覚醒下ヒトを用いた functional OCT の研究にも着手しているが，現時点での信号の質は，信号起源を論じるほどのレベルにはまったく達していない。Functional OCT は信号が小さいうえに，網膜内では光異性化に伴う早い反応から，血流増加に伴う遅い反応まで，起源を異にする信号が隣接する各層から惹起され，非常に複雑な光散乱変化が起きていることが予想される。Functional OCT を臨床的に意味のある検査法とするためには，まず麻酔下のより統制のとれた実験系を用いて，functional OCT でどのような生理学的現象が捉えられているのかを徹底的に調べ上げる必要がある。

Functional OCT の実用化は可能か

可能であろう。ただし，臨床現場での応用を数年以内に実現するのは難しいと思う。例えば LASIK で用いられるようなきわめて高周波数で位置ズレを補正するシステムや，補償光学（adaptive optics）を利用して解像度を上げるシステムも，フラッシュ刺激後にヒトの眼底後極部で起こる微細で複雑な動きに対しては，現状では対処しきれない。また，現在のフーリエドメイン OCT よりもさらに高速のスキャンが可能な次世代 OCT の実用化が待たれているが，それだけでは上述の問題点を解決することはできない。しかし，これらの問題点を 1 つ 1 つクリアしていけば，必ず近い将来にゴールは見えてくるものと筆者らは考えている（図 5）。

文　献

1) Maheswari RU, Takaoka H, Homma R et al：Implementation of optical coherence tomography（OCT）in visualization of functional structures of cat visual cortex. Opt Comm **202**：47-54, 2002
2) Maheswari RU, Takaoka H, Kadono H et al：Novel functional imaging technique from brain surface with optical coherence tomography enabling visualization of depth resolved functional structure in vivo. J Neurosci Methods **124**：83-92, 2003
3) Cohen L：Changes in neuron structure during action potential propagation and synaptic transmission. Physiol Rev **53**：373-418, 1973
4) Harary H, Brown E, Pinto H：Rapid light-induced changes in near infrared transmission of rods in Bufo marinus. Science **202**：1083-1085, 1978
5) Grinvald A, Lieke E, Frostig RD et al：Functional architecture of cortex revealed by optical imaging of intrinsic signals. Nature **324**：361-364, 1986

6) Tsunoda K, Yamane Y, Nishizaki M et al : Complex objects are represented in macaque inferotemporal cortex by the combination of feature columns. Nat Neurosci **4** : 832-838, 2001
7) Tsunoda K, Oguchi Y, Hanazono G et al : Mapping cone- and rod-induced retinal responsiveness in macaque retina by optical imaging. Invest Ophthalmol Vis Sci **45** : 3820-3826, 2004
8) Hanazono G, Tsunoda K, Shinoda K et al : Intrinsic signal imaging in macaque's retina reveals different types of flash-induced light reflectance changes of different origins. Invest Ophthalmol Vis Sci **48** : 2903-2912, 2007
9) Inomata K, Tsunoda K, Hanazono G et al : Distribution of retinal responses evoked by trans-scleral electrical stimulation detected by intrinsic signal imaging in macaque monkeys. Invest Ophthalmol Vis Sci **49** : 2193-2200, 2008
10) Hanazono G, Tsunoda K, Kazato Y et al : Evaluating neural activity of retinal ganglion cells by flash-evoked intrinsic signal imaging in macaque retina. Invest Ophthalmol Vis Sci (in press)
11) Bizheva K, Pflug R, Hermann B et al : Optophysiology : depth-resolved probing of retinal physiology with functional ultrahigh-resolution optical coherence tomography. Proc Natl Acad Sci USA **103** : 5066-5071, 2006
12) Srinivasan VJ, Wojtkowski M, Fujimoto JG et al : In vivo measurement of retinal physiology with high-speed ultrahigh-resolution optical coherence tomography. Opt Lett **31** : 2308-2310, 2006

脳と眼のサイエンス

東京医療センター感覚器センター視覚生理学研究室 角田 和繁

KEY WORDS
●脳科学
●視覚
●可塑性
●経角膜網膜電気刺激

はじめに

人の脳が外界から受けとる情報のうちかなりの部分を視覚情報が占めており，近年の脳科学の発展は視覚研究とともに発達してきたといっても過言ではない。現在でも，脳神経生理学の研究は視覚を通じて行われるものが多く，視覚あるいは眼を研究することは脳，さらには人間そのものの探求にもつながることになる。逆に，大脳生理学で築き上げられた知識や技術が眼科臨床において応用される可能性もあるわけであり，最近の新しい治療法のなかにはこれまでの常識をくつがえす理論に基づくものが散見される。

今回は，中枢神経の可塑性が話題となるなか，眼科領域で試行されすでに良好な結果を得ている視神経の電気刺激治療について述べてみたい。

Ⅰ．中枢神経の可塑性

生後，脳は外界の環境に適応しながら過剰な神経回路の再編成を行い，必要かつ効率のよい神経回路網が次第に固定されていく。これを脳の発達可塑性と呼び，その重要性を示す身近な例として片眼遮蔽による弱視の形成，およびその後の健眼遮蔽による視機能の回復がある[1]。たとえば遠視などの屈折異常により幼児期に片眼の視覚入力が弱められると，外側膝状体や後頭葉視覚野の神経回路が十分に形成されず，網膜や視神経には異常がないにもかかわらず視力が出ない，いわゆる弱視の状態に陥る。しかし早期に健眼遮蔽と屈折矯正治療を行うことで，視機能は正常にまで回復しうる。

これとは別に，発達期を過ぎた脳においても可塑性はみられ，小脳の長期抑圧(LTD)や海馬の長期増強(LTP)などに代表されるシナプス伝達の可塑性が有名である。一方サルの指趾切断後にみられる体性感覚野の体部位再現変化で明らかなように，後天的な損傷などによっても神経回路が再構築されるような可塑性が観察されることがあ

Brain science and vision research
Kazushige Tsunoda(室長)

る[2]。また視覚野においても，両眼の網膜にレーザー凝固を行い人工的に視野欠損を作成すると，大脳皮質第一次視覚野のうち網膜障害部位から入力を受けていた領域の神経細胞が，障害部位以外の視野の視覚刺激に対してもスパイク応答を出すようになる。これは水平方向のニューロンが短期間のうちに機能的に再構築されることを示している[3]。これらの知見をもとに，米国においては脳梗塞後の上肢麻痺に対して，機能回復を目的とした大脳皮質電気刺激療法なども試みられている。

さて，網膜の神経活動を外側膝状体に伝える視神経は中枢神経と同じ性質をもち，一度損傷したら再生はしないと考えられている。しかしFukudaらは，切断したネコの視神経を坐骨神経とつなぎ合わせたところ，視神経の線維が坐骨神経を通って軸索を伸ばし，新たな回路を形成するばかりでなく，光に対する感受性も獲得したことを示している[4]。

Ⅱ．電気刺激による視神経の機能回復治療

網膜神経節細胞は10層構造をもつ網膜の最内層に位置する第三次ニューロンである。視細胞，双極細胞から伝達した信号をスパイク電位に変換し，視覚情報を外側膝状体から脳に伝える役割をもつ。一方，網膜神経節細胞は網膜のなかではその数が特に少なく（ヒトで約100万個），虚血性変化や眼圧変化にきわめて弱いため，さまざまな病態でその機能が低下し視力低下や視野欠損をきたす結果となる。特に，緑内障，非動脈炎型虚血性視神経症，腫瘍による圧迫性視神経症，外傷性視神経症などでは，網膜神経節細胞の細胞死が原因で視野欠損が生じており，１度失われた視野は２度と回復しないというのがこれまでの眼科学の常識であった。

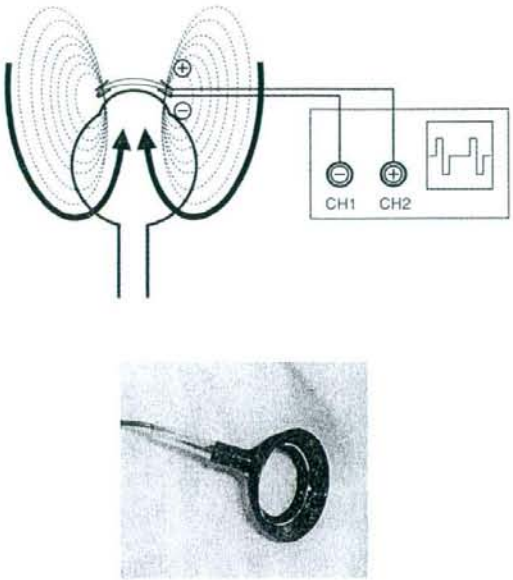

図１．TES治療の模式図
通電用角膜コンタクトレンズ（下）を装着して，眼球内に二相性電流を流す。

これに対して大阪大学のFujikadoらは，視神経に対する電気刺激が軸索を切断された網膜神経節細胞に神経保護効果を生むことをラットによる実験で証明した。すなわち，視神経を切断したラットに対して経角膜的に電気刺激を与えたところ（TES；transcorneal electrical stimulation），電気刺激を行わない網膜に比べてより多くの網膜神経節細胞が生存していた[5]。さらにTESによって神経保護因子であるIGF-１の産生がミュラー細胞において増強していることが示され，これによって網膜電気刺激による視神経疾患の治療への可能性が開かれた[6]。その成果はさっそく視野欠損をきたした患者の治療に応用され，外傷性視神経症および非動脈炎型虚血性視神経症の患者に対して行ったTES治療により，一部の例で視力または視野の改善が得られた[7]。

われわれもこの成果をもとに，2004年より慶應義塾大学病院の倫理委員会の承認を得て，従来の治療法でまったく改善のみられなかった虚血性網膜疾患患者に対して治療目的の網膜電気刺激を行った（図１）。方法はFujikadoらの原法にほぼ準じ，点眼麻酔下にてコンタクトレンズを装着し，疑似光覚（electrical phosphene）を感じ始める程度の電流（1,000 μA以下，20Hz）を30分間通電した。それを月に１回程度継続したところ，陳旧性網膜中心動脈閉塞症および分枝動脈閉塞症の患者において，自覚的所見（視力，視野）の改善

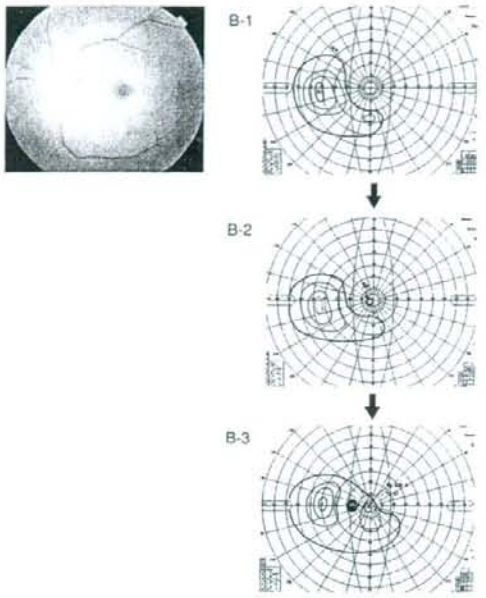

図2．発症後約3年を経過し，症状の固定した陳旧性網膜中心動脈閉塞症患者におけるTES治療経過(60歳男性)[8]
A：発症直後の左眼底写真。
B：治療前後のゴールドマン視野。1は電気刺激施行前，2は1回施行後，3は3回目終了後。電気刺激施行後に中心視野が出現し，視力は0.09から0.15へと改善した。

のみならず，網膜電図(ERG)，多局所網膜電図(mfERG)などの他覚的所見が治療後に改善していることが確認された(図2)[8]。

これらの治療法はその機序にまだ不明な点もあり，一般的な治療法として広くコンセンサスを得るには至っていない。特に今後は，高い治療効果を得るための適応疾患・ステージの選別，通電時間・治療頻度などのプロトコールの設定や，視力・視野検査などの自覚的検査に頼らない，客観的検査法による治療前後の視機能評価が課題となっている。しかし，電気刺激を利用した治療はこれまでに治癒不可能であった視神経の機能障害を改善する画期的な試みであり，今後さらにさまざまな疾患に応用される可能性がある。

おわりに

最近Morimotoらは，網膜変性症のモデルであるRCSラットにTESを施行すると網膜視細胞が機能的にも解剖学的にもより長期に温存されることを示している[9]。眼科学においては新しい神経生理学的な知見をもとにこれまでの常識をくつがえす治療が応用される機会が多く，最新の脳科学とともに進化していくホットな領域である。

文　献

1) Hubel DH, Wiesel TN：The period of susceptibility to the physiological effects of unilateral eye closure in kittens. J Physiol 206：419－436, 1970
2) Merzenich MM, Nelson RJ, Stryker MP, et al：Somatosensory cortical map changes following digit amputation in adult monkeys. J Comp Neurol 224：591－605, 1984
3) Das A, Gilbert CD：Long-range horizontal connections and their role in cortical reorganization revealed by optical recording of cat primary visual cortex. Nature 375：780－784, 1995
4) Fukuda Y, Watanabe M, Sawai H, et al：Functional recovery of vision in regenerated optic nerve fibers. Vision Res 38：1545－1553, 1998
5) Morimoto T, Miyoshi T, Fujikado T, et al：Electrical stimulation enhances the survival of axotomized retinal ganglion cells *in vivo*. Neuroreport 13：227－230, 2002
6) Morimoto T, Miyoshi T, Matsuda S, et al：Transcorneal electrical stimulation rescues axotomized retinal ganglion cells by activating endogenous retinal IGF-1 system. Invest Ophthalmol Vis Sci 46：2147－2155, 2005
7) Fujikado T, Morimoto T, Matsushita K, et al：Effect of transcorneal electrical stimulation in patients with nonarteritic ischemic optic neuropathy or traumatic optic neuropathy. Jpn J Ophthalmol 50：266－273, 2006
8) Inomata K, Shinoda K, Ohde H, et al：Transcorneal electrical stimulation of retina to treat longstanding retinal artery occlusion. Graefes Arch Clin Exp Ophthalmol 245：1773－1780, 2007
9) Morimoto T, Fujikado T, Choi JS, et al：Transcorneal electrical stimulation promotes the survival of photoreceptors and preserves retinal function in royal college of surgeons rats. Invest Ophthalmol Vis Sci 48：4725－4732, 2007

Mini-Symposium

Fine-Scale Spatial Organization of Face and Object Selectivity in the Temporal Lobe: Do Functional Magnetic Resonance Imaging, Optical Imaging, and Electrophysiology Agree?

Hans P. Op de Beeck,[1] James J. DiCarlo,[2]* Jozien B. M. Goense,[3]* Kalanit Grill-Spector,[4]* Alex Papanastassiou,[2]* Manabu Tanifuji,[5]* and Doris Y. Tsao[6,7]*

[1]Laboratory of Experimental Psychology, University of Leuven (Katholieke Universiteit Leuven), B-3000 Leuven, Belgium, [2]McGovern Institute for Brain Research, Massachusetts Institute of Technology, Cambridge, Massachusetts 02139, [3]Max Planck Institute for Biological Cybernetics, 72076 Tuebingen, Germany, [4]Department of Psychology and Neurosciences Institute, Stanford University, Stanford, California 94305, [5]Laboratory Integrative Neural Systems, Riken Brain Science Institute, Saitama 351-0198, Japan, [6]Institute for Brain Research, D-28359 Bremen, Germany, and [7]Division of Biology, California Institute of Technology, Pasadena, California 91125

The spatial organization of the brain's object and face representations in the temporal lobe is critical for understanding high-level vision and cognition but is poorly understood. Recently, exciting progress has been made using advanced imaging and physiology methods in humans and nonhuman primates, and the combination of such methods may be particularly powerful. Studies applying these methods help us to understand how neuronal activity, optical imaging, and functional magnetic resonance imaging signals are related within the temporal lobe, and to uncover the fine-grained and large-scale spatial organization of object and face representations in the primate brain.

Key words: face perception; object recognition; single unit; local field potential; optical imaging; fMRI

Primates have a great capacity to categorize and identify faces and other objects. No artificial intelligent device has ever been created with the same object recognition capabilities as the human brain, despite the speed of modern-day computers. The details of how the primate brain accomplishes this task are still not well known, but we know where to look: the temporal lobe of the brain. Interest in the functional properties of regions in the temporal lobe has been increasing ever since early primate lesion studies showed its importance for learning and object recognition (Dean, 1976). Regretfully, the location of the temporal lobe at the ventral side of the brain makes it cumbersome to access with invasive techniques. In addition, the study of temporal lobe neurons is challenging because these neurons often respond only to a small subset of stimuli. Indeed, most researchers studying the temporal lobe in monkeys have experienced the frustration of investing weeks of time inserting electrodes in this part of the brain before finally finding some recording positions where neurons respond strongly to the visual images included in the experiment. So the importance of understanding functional organization in the temporal lobe is abundantly clear from a practical point of view, but most importantly, it would help us to understand the neural mechanisms behind the superior recognition performance at the behavioral level.

Here, we will focus on several techniques, invasive and noninvasive, and their application in the temporal lobe. To address questions of brain organization, we have several methods at our disposal, including electrophysiology, optical imaging, and functional magnetic resonance imaging (fMRI). In humans, mostly the noninvasive methods are relevant. Two parameters are important for assessing the usefulness of each technique: spatial resolution and coverage. Electrophysiological, extracellular recordings provide single-neuron spatial resolution but focus on a small, potentially unrepresentative local sample of neurons, and optical imaging provides tens of micrometer resolution and a coverage of a few millimeters. For fMRI, the spatial resolution depends on coverage. The spatial resolution is typically a few millimeters for whole-brain studies, but for localized fMRI or in small animals resolution can be 200 μm or less (Fukuda et al., 2006; Harel et al., 2006; Goense et al., 2007).

The first studies investigating the relationships between these techniques have focused on primary visual cortex (V1). The function and organization of this region is so well known from electrophysiology that this area can be used as a test bed for validating new techniques. V1 data showed early on how columns defined by optical imaging relate to extracellular spiking activity (Grinvald et al., 1986). Likewise, orientation columns identified through contrast-enhanced fMRI correspond to orientation columns visualized with optical imaging (Fukuda et al., 2006). Fur

Received Aug. 11, 2008; accepted Sept. 10, 2008.

This work was supported by Human Frontier Science Program Grant CDA-0040/2008 (H.P.O.d.B.); the Fund for Scientific Research–Flanders (H.P.O.d.B.), The Pew Charitable Trusts (UCSF 2893sc) (J.J.D.), The Max Planck Society (J.B.M.G.), Whitehall Foundation Grant 2005-05-111-RES (K.G.-S.), and The Humboldt Foundation (D.Y.T.).

*J.J.D., J.B.M.G., K.G.-S., A.P., M.T., and D.Y.T. contributed equally to this work.

Correspondence should be addressed to Hans P. Op de Beeck, Laboratory of Experimental Psychology, Katholieke Universiteit Leuven, Tiensestraat 102, B-3000 Leuven, Belgium. E-mail: hans.opdebeeck@psy.kuleuven.be.

DOI:10.1523/JNEUROSCI.3799-08.2008

 0270-6474/08/2811796-06$15.00/0

thermore, V1 data demonstrated that the fMRI signal obtained from the intrinsic blood oxygenation level-dependent (BOLD) contrast is slightly better correlated with an indirect measure of synaptic activity [local field potentials (LFPs)] than with multiunit spiking activity (MUA) (Logothetis et al., 2001).

Here, we are not so much interested in the relationships between these techniques per se, but in how the combination of these techniques can help us to clarify the functional organization of regions in the temporal lobe. Our understanding of this functional organization is growing steadily, but is still not sufficient to address the big question of how the spatial organization of the temporal lobe relates to its functional role in visual object recognition. One hypothesis is that there are domain-specific systems containing neurons and circuitry for classes of complex objects such as faces, bodies, etc. Another hypothesis is that there is alphabet of small columns where neurons inside each column prefer a particular feature and the active combination of columns represents each object. A third possibility is that neurons that participate in representing the same object are fully intermixed, perhaps organized into multiple interleaved feature maps.

Here, we will focus on how the combination of electrophysiological and imaging techniques can help unravel the functional organization of the temporal lobe. We will first briefly describe what each technique in isolation has revealed and then we will illustrate the power of their combination. In comparing across techniques, we will address two central questions. First, what are the processes that contribute to the signal measured with each of these methods? Although positive correlations have been found between the different methods, these correlations are smaller than expected given the reliability of the data. This opens the possibility that different methods measure different signals, for example, a differently weighted contribution of the input and the output of neurons. Second, what is the degree and spatial scale of clustering of neurons with similar properties in the temporal lobe? The answers from different techniques (e.g., optical imaging vs fMRI) and different designs (e.g., use of different stimuli) are qualitatively similar, but quantitatively different.

Electrophysiology in monkeys

Gross et al. (1969, 1972) gave an early, qualitative description of neural receptive fields and response properties of neurons in primate inferior temporal (IT) cortex, suggesting cells with relatively large receptive fields that are selective for complex visual stimuli like faces and hands. Decades later, these findings are still valid, although significant research has quantified and qualified these response properties of IT neurons. Many IT neurons are activated strongly by relatively complex stimuli (Perrett et al., 1982; Desimone et al., 1984), but these stimuli are often moderately complex visual features or object fragments rather than images of whole objects (Kobatake and Tanaka, 1994). Furthermore, although this stimulus selectivity is largely tolerant to image transformations like changes in position and size (Ito et al., 1995; Wallis and Rolls, 1997), single neurons nevertheless retain a surprising degree of sensitivity for such transformations (Op de Beeck and Vogels, 2000; DiCarlo and Maunsell, 2003). Computational work and population analyses of neuronal selectivity suggest that a representation of moderately complex features that is largely tolerant for metric transformations like size and position may be an effective population code allowing for invariant object recognition (Hung et al., 2005; DiCarlo and Cox, 2007). Absolute invariance and selectivity for whole objects are not necessary.

The functional organization of IT cortex is another question that has attracted much interest. Are there feature, object, or category columns/maps in IT cortex analogous to orientation columns in V1 or motion-direction maps in MT? Early single-unit electrophysiological studies suggested some clustering (Desimone and Gross, 1979; Gochin et al., 1991), but nevertheless the similarity in response properties between nearby neurons was not very high. Electrophysiology studies have also investigated regional variations in stimulus preference on a larger scale. Most notably, Baylis et al. (1987) described some regional variation in the preference for simple visual stimuli, more complex visual stimuli, and faces, but this variation was relatively modest. Fujita et al. (1992) showed the existence of a finer columnar organization with respect to the simplest visual stimuli that activate neurons efficiently (the "critical features"). A critical feature for a neuron was determined by simplifying the effective stimulus little by little without changing evoked responses of the neuron (the reduction technique). The resulting moderately complex features were similar across nearby neurons and neurons with similar preferences seemed to be organized in a columnar manner in IT cortex. The connectivity within IT cortex (between areas TEO and TE) and afferent input to IT cortex also suggests a columnar organization at a size of a few hundred micrometers (Saleem et al., 1993; Tanigawa et al., 2005).

One question is why the reduction technique proved so useful for finding clustering of neurons with similar properties, while at the same time it is not uncommon to find nearby neurons with a totally different selectivity. One possibility is that the reduction technique partially removes the effects of the intrinsic circuit (e.g., interneurons and horizontal connections) that determines how an IT neuron responds to the afferent input, and so the effect of the afferent input would be greater using the reduction technique than when using more complex stimuli. From this respect, the reduction technique might inform us what the common input is of the neurons in an IT column. Two other methods have also been successful in reducing the variability between IT neurons. First, recent studies have focused on LFPs, which might be related more to synaptic activity than to spiking output. Second, measurements of multiunit activity (instead of single-unit activity) average out the variability across neurons in the local neuronal population. The latter two methods have recently provided evidence for clustering over a distance <500 μm for multiunit activity and over a distance of >1 mm for LFPs (Kreiman et al., 2006). Thus, there appear to be multiple scales and strengths of organization depending on the methodology used and signal that is measured.

Optical imaging in monkeys

Activation in neural tissues elicits changes in optical properties of the tissue. Optical imaging, more specifically optical intrinsic signal imaging (OISI), is a technique to visualize these changes (intrinsic signals) from an exposed cortical surface with CCD cameras. Typically, a wavelength of light ~610 nm is used for measurements of the intrinsic signals in IT cortex. The major source of the changes at this wavelength is the absorption changes reflecting increase of deoxyhemoglobin in capillaries due to increased neural activity. Other sources involved in OISI, such as an increase in absorption due to increases in blood volume in capillaries or changes in light scattering due to microstructural changes in neural tissues, do not dominate at this wavelength.

The presentation of any visual stimulus induces increases of intrinsic signals over an area of several millimeters (global signals), but local signals that spread only for ~0.5 mm are detected

when the intrinsic signals for each stimulus condition is divided by the mean of intrinsic signals elicited by many stimuli (Wang et al., 1996, 1998) or by removing the global signals with spatial filtering (Tsunoda et al., 2001). The stimulus specific local signals (activity spots) are considered as supporting evidence for the existence of feature columns in IT cortex. Correlation between spiking activity of single cells and spot activity was examined in two ways. First, OISI with the critical stimulus features that were predetermined from spiking activity of single neurons revealed optical activity spots at the location where the single neurons were recorded (Wang et al., 1996, 1998). Second, selectivity of neural firing in activity spots was well correlated with selectivity of local optical signals at the spots (Tsunoda et al., 2001). Thus, spiking activity of neurons is well correlated in stimulus selectivity and in spatial localization with the local optical signals. It should be pointed out that, because intrinsic signals reflect population (spiking) activity of neurons, the best correlation between the local signals and neuronal firing is obtained at the level of MUA rather than single-unit activity (SUA).

Optical imaging with object images revealed that each object image is represented by the combined activity of multiple activity spots, and each spot represents a visual feature of the complex object image (Tsunoda et al., 2001). Finally, optical imaging with faces revealed that different viewing angles of a face were continuously and systematically mapped on the IT cortex (Wang et al., 1998). This might be part of a general tendency that similar visual features are mapped in nearby locations in IT cortex (Tanaka, 2003).

Human and monkey fMRI

Most fMRI studies in humans are based on an intrinsic signal, the BOLD contrast, which originates in a mismatch between the blood flow and oxygen extraction of the tissue. This mismatch leads to a net decrease in the concentration of deoxyhemoglobin in veins and capillaries around neuronal activity, which locally increases the magnetic resonance (MR) signal because deoxyhemoglobin acts as an MR contrast agent. In this respect, BOLD fMRI exhibits a striking contrast to OISI. OISI is sensitive to the early increase of deoxyhemoglobin in capillaries, whereas BOLD fMRI is more sensitive to the following oversupply of oxyhemoglobin (causing a decrease in the deoxyhemoglobin concentration) in capillaries and veins.

Even though in many human fMRI studies voxel sizes of 3 mm or larger are used, which are much larger than the size of the feature columns identified in monkey IT with invasive techniques, such studies have revealed surprisingly strong selectivity for comparisons between object classes such as faces versus objects and scenes (Kanwisher et al., 1997), (headless) bodies versus other object categories (Downing et al., 2001), and scenes/buildings versus objects and faces (Epstein and Kanwisher, 1998; Ishai et al., 1999). Similarly, in monkeys BOLD and contrast agent-dependent cerebral blood volume (CBV) images acquired at a resolution of 1.25 mm revealed patches in monkey IT cortex that responded more strongly to faces or body parts than to objects (Tsao et al., 2003; Pinsk et al., 2005; Op de Beeck et al., 2008b). These findings are exciting, not the least because they were unexpected from previous electrophysiology experiments that had not shown large (>1 mm) cortical regions with a strong preference for specific object categories and with a consistent location across subjects.

Recent studies have used high-resolution fMRI (HR-fMRI) as the ultimate solution to better link fMRI to high-resolution optical imaging and electrophysiology data. Data suggest that regions that look like one large homogeneous blob (~1 cm diameter) at standard fMRI resolution can be distinguished into separate regions (Schwarzlose et al., 2005) or even more heterogeneous clusters of voxels (Grill-Spector et al., 2006) at higher fMRI resolution. The difficulty of high-resolution fMRI, however, is that using smaller voxels decreases the signal-to-noise ratio (SNR), and increasing the resolution comes at the risk that (weak) activation may be missed. SNR improvement can be gained via parallel imaging, using high field scanners, or both. For parallel imaging, the sensitivity is improved by using multiple smaller radiofrequency coils (RF) coils. High magnetic fields increase the overall signal-to-noise, and the BOLD signal is also larger at high field. This makes the application of spin-echo (SE) sequences more practicable at high field (Goense et al., 2008). SE sequences have two advantages, compared with the commonly used gradient echo EPI (GE) sequence. SE sequences are less susceptible to signal loss from susceptibility artifacts from the air cavity that plague fMRI of the temporal lobe. Most importantly, SE sequences are thought to provide more localized activations from the capillary bed rather than from larger veins. For example, although ocular dominance columns and orientation columns in cat or human V1 are often difficult to discern with GE imaging, other fMRI methods (SE-BOLD imaging as well as cerebral blood volume/flow imaging) have higher specificity and allow for submillimeter resolution (Duong et al., 2003; Kim et al., 2004; Zhao et al., 2005; Yacoub et al., 2008). Nevertheless, it is yet unknown what is the maximal possible spatial resolution with HR-fMRI. This HR-fMRI limit depends on several factors: (1) signal-to-noise limitations, (2) the point spread function of the BOLD signal (which differs between SE and GE imaging), (3) the spatial scale of the neural clustering, and (4) the spatial scale of the separation between clusters having similar properties.

Many important functional questions remain unresolved given the currently available fMRI evidence. What factors underlie the large-scale selectivity to specific categories (e.g., faces and headless bodies) observed with fMRI? Is the selectivity stronger for these categories than for other categories? Is the spatial scale of representation (clustering of neurons with similar properties) larger and thus more easily measured with fMRI? Does processing of these categories rely on different computations? Is category selectivity related to other characteristics of functional organization? How do these category-selective regions come about? fMRI studies have addressed some of these questions. First, it has been suggested that the strong selectivity for stimuli like faces might be related to their form or shape (Haxby et al., 2000), to specific processing related to faces (i.e., face recognition requires recognition at the exemplar level more than objects) (Gauthier, 2000), to semantic attributes in humans (Chao et al., 1999), and/or to eccentricity biases (Hasson et al., 2002) (regions that prefer faces also have a preference for foveal vs peripheral representations). Furthermore, selectivity in the ventral stream takes more than a decade to reach the adult-like state (Golarai et al., 2007). However, it is yet unclear how the strong selectivity for some object classes is related to these properties or their combination (Op de Beeck et al., 2008a). At the very least, a recent electrophysiological study suggests that the object category structure encoded by the firing rates of IT neurons corresponds to a level of visual form beyond a randomly selected set of moderately complex features (Kiani et al., 2007).

Correspondence between fMRI, optical imaging, and electrophysiology

Previous work in other areas of the brain, most notably primary visual cortex, has focused on the relationship between fMRI, optical imaging, SUA and MUA, and LFPs. fMRI, single-neuron activity, and LFPs tend to correspond rather well in typical situations (Logothetis et al., 2001; Mukamel et al., 2005). This is possibly not that surprising, given that the input to a cluster of neurons is a significant determinant of their output. However, a few studies have been able to disentangle input and output of V1 neurons by manipulating the temporal characteristics of the stimuli. Synaptic activity and LFPs are less sensitive to adaptation (more sustained response to constant stimulation) and the frequency of flicker (nonbaseline response to rapidly flickering stimulus) compared with the spiking output of V1 neurons. In these cases, the fMRI signal seems to correlate more with LFPs than with the spiking output (Logothetis et al., 2001; Lauritzen, 2005; Viswanathan and Freeman, 2007). Dissociation between fMRI/LFP and spiking activity can also be induced with pharmacological manipulations that specifically affect the spiking output (Rauch et al., 2008). However, the correlation between spikes and LFP may depend on the degree of intercorrelations between the firing of neurons, and there is still some controversy about the exact relationship between these signals (Nir et al., 2008; Viswanathan and Freeman, 2008).

Here, we are mainly interested in the correspondence between these signals across spatial locations. A first point of consideration is the resolution and spatial spread of each technique. MUA and SUA sample the output of neurons, whereas LFP is a weighted signal dominated by dendritic input (Logothetis, 2003). MUA and SUA have highest spatial resolution, whereas LFPs are correlated across larger distances, often larger than feature columns or ocular dominance or orientation columns in V1. In V1, the spatial spread of LFP signals is of the order of a few millimeters (Juergens et al., 1999; Goense and Logothetis, 2008), whereas in IT the LFP signal spans a larger region, ~5–8 mm (Kreiman et al., 2006). In IT, LFPs were correlated across sites with a much larger distance than multiunit activity, and in addition LFP selectivity could not be predicted very well from multiunit activity averaged across sites with varying diameter (Kreiman et al., 2006). This confirms that LFP represents also in IT a different signal than the MUA. Because the spatial extent of LFP is apparently larger than the spatial specificity of the local optical imaging signals, it is unclear how the specificity of the LFP relates to the specificity of the hemodynamic signals (optical imaging and fMRI).

Because optical imaging and fMRI both measure the hemodynamic response induced by neural activity, the two techniques should show similar results, as indeed they do in V1, in which correspondence was found between orientation columns measured by optical imaging and contrast agent-enhanced fMRI (Fukuda et al., 2006). This demonstration involved very high-field scanning (9.4 T) and contrast agent-enhanced CBV-weighted fMRI in cats, as well as analysis techniques that allowed removal of potentially existing global nonselective signals. As mentioned above, GE-BOLD fMRI might lack sufficient spatial specificity to show a similar correspondence. Similar experiments are not straightforward in primate IT, because typically the effective fMRI resolution is lower (2 mm) and the spots seen in optical imaging are not larger than in cat V1. At current fMRI resolutions, we expect to get a weighted average of the spots/feature columns within a voxel, which may fall apart as the resolution increases. The reported fMRI selectivity for unfamiliar shapes in monkey IT cortex (Op de Beeck et al., 2008b) might reflect such subsampling of very selective feature columns, but higher-resolution scanning is needed to test this hypothesis.

Many unknowns exist about the degree of correspondence between the invasive techniques and fMRI, but some correspondence is definitely present. For example, in monkeys it has been shown that fMRI-identified face-selective patches in the temporal lobe (six per hemisphere) contain a striking majority of neurons that are face-selective (Tsao et al., 2006). Functional connectivity experiments have already revealed the connectivity of the six face patches (Moeller et al., 2008), and electrophysiological experiments might pinpoint the unique step in face recognition performed by each of the different face patches.

However, many questions remain. First of all, faces may be a special category of stimuli, and we can question how these findings translate to other object categories. Furthermore, the properties of the fMRI-identified face patches have not been exhaustively compared with the properties of patches and columns as defined electrophysiologically through a dense sampling of single-unit activity both inside and outside the fMRI-identified face patches. Although the currently available evidence is very suggestive that face-selective patches have different properties than feature columns, a definitive answer awaits a better understanding of the functional and anatomical properties of both patches and columns. Finally, it is nontrivial to compare results across species. Homology of regions across species beyond early sensory areas is complex and often debatable (Kaas, 2008); the spatial scale of structures may differ across species (Adams et al., 2007). Furthermore, performing equivalent experiments across species is difficult even with fMRI. For example, should the comparison of face-selective responses across species use the same stimuli (e.g., human faces) or conspecific stimuli (human faces for humans and monkey faces for macaques)?

Conclusion

We are far from a complete understanding of the fine-scale and large-scale spatial organization of the cortical regions important for object and face recognition. Nevertheless, we have already experienced the power of a combined application of multiple neuroscientific techniques that measure functional organization at different spatial scales.

Ultimately, we apply these methods in the temporal lobe to understand how the brain recognizes and categorizes objects. The spatial organization of object representations is only one part of this general question, and it is the part for which the combined application of these neuroscientific techniques is most useful. However, neighboring single neurons often have clearly different selectivity properties and functions. Such differences are necessarily confounded, and underestimated, by techniques that pool signals over larger numbers of neurons, such as optical imaging and fMRI. Thus, the "gold standard" for understanding neural mechanisms remains single-unit electrophysiology. Nevertheless, the coarser-scale techniques can reveal large-scale patterns of organization that would otherwise go undetected, thereby helping single-unit electrophysiologists to target their electrodes better. In addition, the noninvasive techniques allow comparison between human and nonhuman brains, thereby providing a strong test of human–monkey correspondences and even allowing human studies to lead targeted electrophysiological experiments.

There are several outstanding questions that will only be solved by the combined application of all these methods, direct in the same study or indirect in different studies/laboratories. These

questions center on the relationships between the different methods, the factors that underlie spatial organization in the temporal lobe at multiple scales, and how this multiple-scale organization emerges in the light of plasticity during development and adulthood. At a very basic level, we still do not know why we see clustering for particular functional properties (e.g., does the clustering of face cells in patches contribute to the speed and efficiency of face recognition?). Answering questions like this one will bring us closer to a full understanding of how the spatial organization of the temporal lobe relates to its functional role in visual object and face recognition.

References

Adams DL, Sincich LC, Horton JC (2007) Complete pattern of ocular dominance columns in human primary visual cortex. J Neurosci 27:10391–10403.

Baylis GC, Rolls ET, Leonard CM (1987) Functional subdivisions of the temporal lobe neocortex. J Neurosci 7:330–342.

Chao LL, Haxby JV, Martin A (1999) Attribute based neural substrates in temporal cortex for perceiving and knowing about objects. Nat Neurosci 2:913–919.

Dean P (1976) Effects of inferotemporal lesions on the behavior of monkeys. Psychol Bull 83:41–71.

Desimone R, Gross CG (1979) Visual areas in the temporal cortex of the macaque. Brain Res 178:363–380.

Desimone R, Albright TD, Gross CG, Bruce C (1984) Stimulus selective properties of inferior temporal neurons in the macaque. J Neurosci 4:2051–2062.

DiCarlo JJ, Cox DD (2007) Untangling invariant object recognition. Trends Cogn Sci 11:333–341.

DiCarlo JJ, Maunsell JH (2003) Anterior inferotemporal neurons of monkeys engaged in object recognition can be highly sensitive to object retinal position. J Neurophysiol 89:3264–3278.

Downing PE, Jiang Y, Shuman M, Kanwisher N (2001) A cortical area selective for visual processing of the human body. Science 293:2470–2473.

Duong TQ, Yacoub E, Adriany G, Hu X, Ugurbil K, Kim SG (2003) Microvascular BOLD contribution at 4 and 7 T in the human brain: gradient-echo and spin-echo fMRI with suppression of blood effects. Magn Reson Med 49:1019–1027.

Epstein R, Kanwisher N (1998) A cortical representation of the local visual environment. Nature 392:598–601.

Fujita I, Tanaka K, Ito M, Cheng K (1992) Columns for visual features of objects in monkey inferotemporal cortex. Nature 360:343–346.

Fukuda M, Moon CH, Wang P, Kim SG (2006) Mapping iso-orientation columns by contrast agent-enhanced functional magnetic resonance imaging: reproducibility, specificity, and evaluation by optical imaging of intrinsic signal. J Neurosci 26:11821–11832.

Gauthier I (2000) What constrains the organization of the ventral temporal cortex? Trends Cogn Sci 4:1–2.

Gochin PM, Miller EK, Gross CG, Gerstein GL (1991) Functional interactions among neurons in inferior temporal cortex of the awake macaque. Exp Brain Res 84:505–516.

Goense JB, Logothetis NK (2008) Neurophysiology of the BOLD fMRI signal in awake monkeys. Curr Biol 18:631–640.

Goense JB, Zappe AC, Logothetis NK (2007) High-resolution fMRI of macaque V1. Magn Reson Imaging 25:740–747.

Goense JB, Ku SP, Merkle H, Tolias AS, Logothetis NK (2008) fMRI of the temporal lobe of the awake monkey at 7 T. Neuroimage 39:1081–1093.

Golarai G, Ghahremani DG, Whitfield-Gabrieli S, Reiss A, Eberhardt JL, Gabrieli JD, Grill-Spector K (2007) Differential development of high-level visual cortex correlates with category-specific recognition memory. Nat Neurosci 10:512–522.

Grill-Spector K, Sayres R, Ress D (2006) High-resolution imaging reveals highly selective nonface clusters in the fusiform face area. Nat Neurosci 9:1177–1185.

Grinvald A, Lieke E, Frostig RD, Gilbert CD, Wiesel TN (1986) Functional architecture of cortex revealed by optical imaging of intrinsic signals. Nature 324:361–364.

Gross CG, Bender DB, Rocha-Miranda CE (1969) Visual receptive fields of neurons in inferotemporal cortex of the monkey. Science 166:1303–1306.

Gross CG, Rocha-Miranda CE, Bender DB (1972) Visual properties of neurons in inferotemporal cortex of the macaque. J Neurophysiol 35:96–111.

Harel N, Lin J, Moeller S, Ugurbil K, Yacoub E (2006) Combined imaging-histological study of cortical laminar specificity of fMRI signals. Neuroimage 29:879–887.

Hasson U, Levy I, Behrmann M, Hendler T, Malach R (2002) Eccentricity bias as an organizing principle for human high-order object areas. Neuron 34:479–490.

Haxby JV, Ishai H, Chao LL, Ungerleider LG, Martin I (2000) Object-form topology in the ventral temporal lobe. Response to I. Gauthier (2000). Trends Cogn Sci 4:3–4.

Hung CP, Kreiman G, Poggio T, DiCarlo JJ (2005) Fast readout of object identity from macaque inferior temporal cortex. Science 310:863–866.

Ishai A, Ungerleider LG, Martin A, Schouten JL, Haxby JV (1999) Distributed representation of objects in the human ventral visual pathway. Proc Natl Acad Sci U S A 96:9379–9384.

Ito M, Tamura H, Fujita I, Tanaka K (1995) Size and position invariance of neuronal responses in monkey inferotemporal cortex. J Neurophysiol 73:218–226.

Juergens E, Guettler A, Eckhorn R (1999) Visual stimulation elicits locked and induced gamma oscillations in monkey intracortical- and EEG-potentials, but not in human EEG. Exp Brain Res 129:247–259.

Kaas JH (2008) The evolution of the complex sensory and motor systems of the human brain. Brain Res Bull 75:384–390.

Kanwisher N, McDermott J, Chun MM (1997) The fusiform face area: a module in human extrastriate cortex specialized for face perception. J Neurosci 17:4302–4311.

Kiani R, Esteky H, Mirpour K, Tanaka K (2007) Object category structure in response patterns of neuronal population in monkey inferior temporal cortex. J Neurophysiol 97:4296–4309.

Kim DS, Ronen I, Olman C, Kim SG, Ugurbil K, Toth LJ (2004) Spatial relationship between neuronal activity and BOLD functional MRI. Neuroimage 21:876–885.

Kobatake E, Tanaka K (1994) Neuronal selectivities to complex object features in the ventral visual pathway of the macaque cerebral cortex. J Neurophysiol 71:856–867.

Kreiman G, Hung CP, Kraskov A, Quiroga RQ, Poggio T, DiCarlo JJ (2006) Object selectivity of local field potentials and spikes in the macaque inferior temporal cortex. Neuron 49:433–445.

Lauritzen M (2005) Reading vascular changes in brain imaging: is dendritic calcium the key? Nat Rev Neurosci 6:77–85.

Logothetis NK (2003) The underpinnings of the BOLD functional magnetic resonance imaging signal. J Neurosci 23:3963–3971.

Logothetis NK, Pauls J, Augath M, Trinath T, Oeltermann A (2001) Neurophysiological investigation of the basis of the fMRI signal. Nature 412:150–157.

Moeller S, Freiwald WA, Tsao DY (2008) Patches with links: a unified system for processing faces in the macaque temporal lobe. Science 320:1355–1359.

Mukamel R, Gelbard H, Arieli A, Hasson U, Fried I, Malach R (2005) Coupling between neuronal firing, field potentials, and FMRI in human auditory cortex. Science 309:951–954.

Nir Y, Dinstein I, Malach R, Heeger DJ (2008) BOLD and spiking activity. Nat Neurosci 11:523–524; author reply 524.

Op de Beeck H, Vogels R (2000) Spatial sensitivity of macaque inferior temporal neurons. J Comp Neurol 426:505–518.

Op de Beeck HP, Haushofer J, Kanwisher NG (2008a) Interpreting fMRI data: maps, modules and dimensions. Nat Rev Neurosci 9:123–135.

Op de Beeck HP, Deutsch JA, Vanduffel W, Kanwisher NG, DiCarlo JJ (2008b) A stable topography of selectivity for unfamiliar shape classes in monkey inferior temporal cortex. Cereb Cortex 18:1676–1694.

Perrett DI, Rolls ET, Caan W (1982) Visual neurones responsive to faces in the monkey temporal cortex. Exp Brain Res 47:329–342.

Pinsk MA, DeSimone K, Moore T, Gross CG, Kastner S (2005) Representations of faces and body parts in macaque temporal cortex: a functional MRI study. Proc Natl Acad Sci U S A 102:6996–7001.

Rauch A, Rainer G, Logothetis NK (2008) The effect of a serotonin-induced dissociation between spiking and perisynaptic activity on BOLD functional MRI. Proc Natl Acad Sci U S A 105:6759–6764.

Saleem KS, Tanaka K, Rockland KS (1993) Specific and columnar projection from area TEO to TE in the macaque inferotemporal cortex. Cereb Cortex 3:454–464.

Schwarzlose RF, Baker CI, Kanwisher N (2005) Separate face and body selectivity on the fusiform gyrus. J Neurosci 25:11055–11059.

Tanaka K (2003) Columns for complex visual object features in the inferotemporal cortex: clustering of cells with similar but slightly different stimulus selectivities. Cereb Cortex 13:90–99.

Tanigawa H, Wang Q, Fujita I (2005) Organization of horizontal axons in the inferior temporal cortex and primary visual cortex of the macaque monkey. Cereb Cortex 15:1887–1899.

Tsao DY, Freiwald WA, Knutsen TA, Mandeville JB, Tootell RB (2003) Faces and objects in macaque cerebral cortex. Nat Neurosci 6:989–995.

Tsao DY, Freiwald WA, Tootell RB, Livingstone MS (2006) A cortical region consisting entirely of face-selective cells. Science 311:670–674.

Tsunoda K, Yamane Y, Nishizaki M, Tanifuji M (2001) Complex objects are represented in macaque inferotemporal cortex by the combination of feature columns. Nat Neurosci 4:832–838.

Viswanathan A, Freeman RD (2007) Neurometabolic coupling in cerebral cortex reflects synaptic more than spiking activity. Nat Neurosci 10:1308–1312.

Viswanathan A, Freeman RD (2008) Reply to "BOLD and spiking activity." Nat Neurosci 11:524.

Wallis G, Rolls ET (1997) Invariant face and object recognition in the visual system. Prog Neurobiol 51:167–194.

Wang G, Tanaka K, Tanifuji M (1996) Optical imaging of functional organization in the monkey inferotemporal cortex. Science 272:1665–1668.

Wang G, Tanifuji M, Tanaka K (1998) Functional architecture in monkey inferotemporal cortex revealed by in vivo optical imaging. Neurosci Res 32:33–46.

Yacoub E, Harel N, Ugurbil K (2008) High-field fMRI unveils orientation columns in humans. Proc Natl Acad Sci U S A 105:10607–10612.

Zhao F, Wang P, Hendrich K, Kim SG (2005) Spatial specificity of cerebral blood volume-weighted fMRI responses at columnar resolution. Neuroimage 27:416–424.

Cerebral Cortex Advance Access published December 9, 2008

Cerebral Cortex
doi:10.1093/cercor/bhn238

Cortical Columnar Organization Is Reconsidered in Inferior Temporal Cortex

Takayuki Sato, Go Uchida and Manabu Tanifuji

Laboratory for Integrative Neural Systems, RIKEN Brain Science Institute, Wako-shi, Saitama 351-0198, Japan

The object selectivity of nearby cells in inferior temporal (IT) cortex is often different. To elucidate the relationship between columnar organization in IT cortex and the variability among neurons with respect to object selectivity, we used optical imaging technique to locate columnar regions (activity spots) and systematically compared object selectivity of individual neurons within and across the spots. The object selectivity of a given cell in a spot was similar to that of the averaged cellular activity within the spot. However, there was not such similarity among different spots (>600 μm apart). We suggest that each cell is characterized by 1) a cell-specific response property that cause cell-to-cell variability in object selectivity and 2) one or potentially a few numbers of response properties common across the cells within a spot, which provide the basis for columnar organization in IT cortex. Furthermore, similarity in object selectivity among cells within a randomly chosen site was lower than that for a cell in an activity spot identified by optical imaging beforehand. We suggest that the cortex may be organized in a region where neurons with similar response properties were densely clustered and a region where neurons with similar response properties were sparsely clustered.

Keywords: high-resolution fMRI, inferior temporal, intrinsic signal, local field potential, multiunit activity, object vision

Introduction

Functional imaging techniques such as intrinsic signal imaging and functional magnetic resonance imaging (fMRI) have been widely used to investigate brain functions at the systems level. These techniques allow us to simultaneously record activity widely distributed in the brain. The spatial resolution of these techniques, however, is not as high as that provided by conventional single-cell recordings. Thus, in many cases, it is implicitly assumed that response properties of cells within a minimum cluster detectable by the techniques are similar to each other. To justify these techniques as a tool to elucidate neural functions, it is essential to understand the relationship between single-cell activity and population activity in the minimum detectable cluster. In particular, the commonality of neuronal responses at the columnar level has become progressively important because the techniques have nearly reached the spatial resolution to visualize cortical columns in early sensory areas (Cheng et al. 2001; Fukuda et al. 2006) and in association cortices (Malonek et al. 1994; Wang et al. 1996, 1998; Tsunoda et al. 2001; Baker et al. 2004; Tsao et al. 2006; Yamane et al. 2006).

The existence of columnar organization is well established in primary visual cortex, area MT, and somatosensory cortex (Mountcastle 1957; Hubel and Wiesel 1962; Albright et al. 1984). In other cortical areas including association cortices, early studies also reported some tendency that neurons with similar response properties were clustered together (Gross et al. 1972; Perrett et al. 1984). For example, Gross et al. described in their paper that a cluster of successively recorded neurons in IT cortex responded similarly to visual stimuli (Gross et al. 1972). However, firm evidence for columnar organization in these cortices has not been found, and thus, columnar organization has not been fully established as a universal functional organization principle in cerebral cortices till recently.

After the early studies suggesting columnar organization in association cortices, IT cortex has been one of the target area where columnar organization was investigated systematically (Fujita et al. 1992; Tamura et al. 2005; Kreiman et al. 2006). IT cortex is essential for object recognition and is characterized by 2 types of neurons: neurons that respond to behaviorally important objects, faces, and hands and neurons that respond to visual features that are complex but still less complex than object images (Gross et al. 1972; Desimone et al. 1984; Perrett et al. 1984; Tanaka et al. 1991; Kobatake and Tanaka 1994). The first systematic examination of columnar organization in area TE, a part of IT cortex, was conducted by Fujita et al. (1992). They used a stimulus simplification technique to identify the simplest visual feature (critical features) of one cell and generated a stimulus set including optimal (critical feature), suboptimal, and inefficient stimuli for the cell (for the stimulus simplification technique, see Tanaka et al. 1991; Kobatake and Tanaka 1994). Then, they examined responses to the stimulus set for other cells along the recording track. The results revealed that the other cells also best responded to the critical feature of the first cell or the stimuli nearly the same as the critical feature if the recording track was perpendicular to the cortical surface. On the contrary, however, optimal stimuli of the cells were entirely different from the critical feature of the first cells if they were separated from the first cell by more than 0.4 mm along the track parallel to the cortical surface. These results suggested the existence of columnar organization in IT cortex with respect to "critical features," namely, there is a common property across the cells in a columnar region, and this common property is represented by a critical feature (see Tanaka 1996 for review).

The columnar organization in IT cortex has been also examined through comparison of stimulus selectivity of nearby cells (Gochin et al. 1991; Tamura et al. 2005; Kreiman et al. 2006). For example, in recent 2 studies, stimulus selectivity of isolated cells was examined for 64 (Tamura et al. 2005) and 77 visual stimuli (Kreiman et al. 2006), and the

similarity in stimulus selectivity of 2 recorded cells was quantified by calculating the correlation coefficient between their evoked responses to these stimuli. Tamura et al. reported that the median value of the correlation coefficients was 0.08 for pairs of closely located cells isolated from a single-shaft electrode with multiple recording probes. Kreiman et al. found that the mean value of correlation coefficient was 0.21 ± 0.16 for pairs of isolated neurons recorded within the same penetration tracks that were approximately aligned along the columnar axis (Kreiman et al. 2006; DiCarlo JJ, personal communication). These reports provided evidence for the columnar organization in IT cortex because the values of the correlation coefficients between cells spatially separated tangentially along the cortical surface were much lower than the values indicated above. However, the absolute values of the correlation coefficient shown above (0.08 and 0.2) are too low by themselves as convincing evidence for the columnar organization in IT cortex and seemingly contradict the previous report that suggests columnar organization in IT (see also Fig. 1). Thus, we need to explain these low values of the correlation coefficient to justify the columnar organizations in IT in addition to the relative difference in correlation coefficient values depending on the spatial relationship among the cells.

One possible reason for the low values of the correlation coefficient of stimulus selectivity of nearby cells is that these correlation coefficient values are underestimated by trial-to-trial variation of evoked responses. However, it does not seem to be the case. In the above study, for example, trial-to-trial variation gave 0.5 in correlation coefficients, which is much higher than the correlation coefficient value of stimulus selectivity of 2 cells (Kreiman et al. 2006). An alternative possibility is that the electrode penetrations were not exactly perpendicular to the cortical surface, and thus, the electrodes failed to go through the identical columns. This could be the case particularly when the electrodes were penetrated from the dorsal surface of the brain and traveled a long distance before reaching IT cortex.

Thus, in the present paper, we reexamined columnar organization in IT cortex. To penetrate electrodes to putative columnar regions, we exposed the cortical surface of IT cortex, used optical imaging to find candidate sites for columns, and then penetrated electrodes perpendicular to the cortical surface. Furthermore, instead of using the stimulus simplification technique (which is not an entirely objective technique), we investigated similarity in object selectivity of nearby cells. In brief, we found that each cell is characterized by 2 aspects: 1) a cell-specific response property and 2) one or potentially a few numbers of response properties common across the cells in a columnar region. In the correlation analysis of stimulus selectivity for isolated cell pairs, the cell-specific response property was emphasized, and thus, the correlation coefficient values were low. We suggest that the apparent columnar organization reported in the previous study (Fujita et al. 1992) was a result of their stimulus simplification procedure, which enables extraction of a response property that is common across the cells.

Materials and Methods

General Experimental Conditions

Three hemispheres of 3 macaque monkeys (*Macaca mulatta*) were used in this study. In 2 hemispheres, we conducted intrinsic signal imaging and electrophysiological recording experiments while the monkeys were under anesthesia. In the third hemisphere, we conducted only electrophysiological recordings. The experimental protocol was approved by the Experimental Animal Committee of the RIKEN Institute. All experimental procedures were performed in accordance with the guidelines of the RIKEN Institute and the National Institutes of Health.

Anesthesia

During the initial surgery to implant a head fixation post and a recording chamber, the monkeys were anesthetized with intraperitoneal injection of pentobarbital sodium (35 mg/kg at the beginning and supplemented by an additional 5 mg injected intravenously [i.v.] if necessary). During the intrinsic signal imaging and electrophysiological recording, the monkeys were paralyzed by i.v. injection of vecuronium bromide (0.067 mg/kg/h) and artificially ventilated

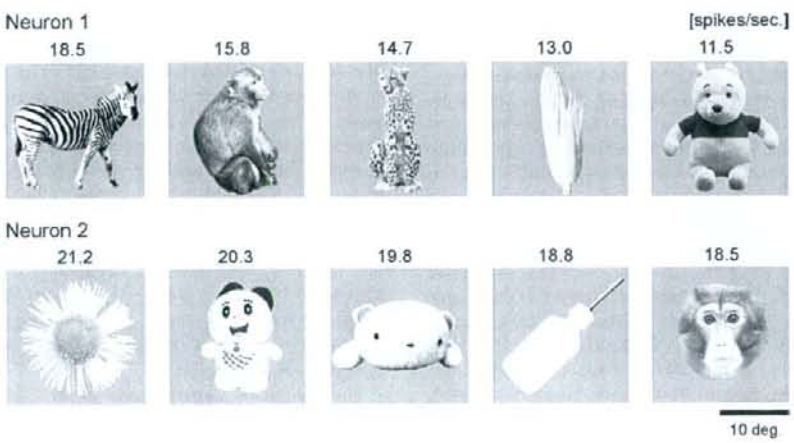

Figure 1. A case showing that the top 5 object stimuli of 2 adjacent isolated neurons were completely different. Each row gives the top 5 visual stimuli for a neuron. For each neuron, these 5 stimuli elicited visual responses stronger than the other 95 object stimuli. The number at each picture indicates the evoked response elicited by the stimulus (spikes/s). These neurons were spaced 150 μm apart. The response similarity between these cells for 100 object stimuli, expressed as a correlation coefficient of evoked responses, was 0.22.

Figure 2. One hundred object stimuli used for examination of object selectivity. The stimuli in the top 2 rows were also used in intrinsic signal imaging sessions.

with a mixture of N_2O, O_2, and isoflurane (70% N_2O, 30% O_2, isoflurane up to 0.5%). In order to remove pain, fentanyl citrate (0.83 μg/kg/h) was infused i.v. and continuously throughout the experiments. Electroencephalography (EEG), electrocardiogram, expired CO_2 concentration, and rectal temperature were monitored throughout the experiments.

Surgical Procedures

In the initial surgery, we implanted the head fixation post and the recording chamber according to a previous study's protocol (Wang et al. 1998). A stainless steel post for the head fixation was attached to the top of the skull. After the attachment, 2 stainless steel bolts for EEG recordings were implanted through the skull above the dural surface of left and right frontal cortices. Finally, the titanium chamber (diameter 22.5 mm) was fixed to the skull at the position corresponding to the dorsal part of area TE. The center of the chamber was placed at 15.0–17.5 mm anterior to the ear bar position. Under this coordination, the anterior middle temporal sulcus was located at the lower center edge of the chamber.

After recovery from the initial surgery, the skull and dura inside the chamber were removed for intrinsic signal imaging and extracellular recording. For intrinsic signal imaging, the chamber was filled with heavy silicon oil (1000 cs) and a glass coverslip was attached to the titanium chamber. For extracellular recordings, the exposed cortex was covered with a transparent artificial dura made of silicon rubber (Arieli et al. 2002). The chamber was filled with 15 mg/ml agarose (Agarose-HGS; Nacalai Tesque, Kyoto, Japan) and covered with a plastic coverslip with a small hole. The electrodes were inserted through the hole. The surface blood vessel pattern was used as a mapping reference for the electrode penetration sites.

Visual Stimuli

Visual stimuli were presented to the eye contralateral to the recording hemisphere. We measured the optics of the eye and focused monkey's eye on a screen of a CRT monitor placed 57 cm from the eye using a contact lens. Fundus photography was taken to determine the position of the fovea.

In this study, we used 100 complex object images as visual stimuli (Fig. 2). To avoid bias among these stimuli, we chose stimuli from different categories, such as fruits and vegetables, plants, tools, animals, stuffed animals, and insects. These visual stimuli were presented on the 21-inch CRT display. The stimuli were centered at the position of the

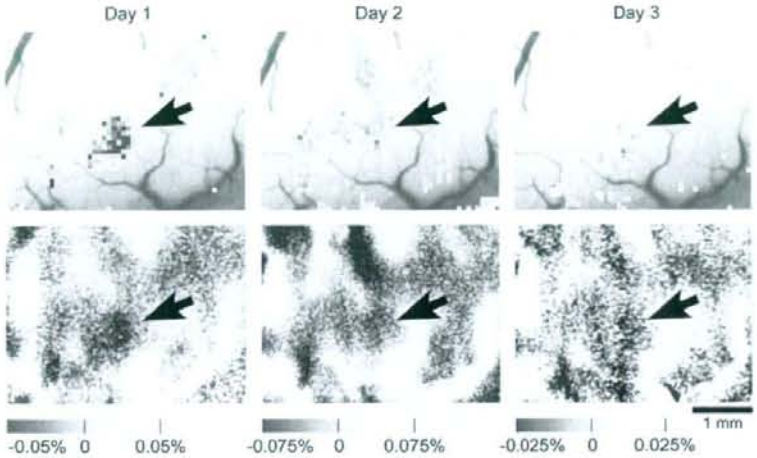

Figure 3. Reproducible responses of intrinsic signals to an object stimulus. Upper panels indicate regions in which the reflection increases elicited by the stimulus were significantly greater than the increases of reflection caused by spontaneous fluctuation. The highest significance level is denoted by red and the lowest by yellow where $P < 0.05$ (*t*-test). Lower panels indicate reflection changes of the cortex elicited by visual stimulus presentation (see Tsunoda et al. 2001 for details). Horizontal scales represent percent changes in reflection. The optical responses at the first, second, and third days are represented from left to right. The arrow indicates reproducible active spots. The stimulus that elicited the activation was the upper-left object image in Figure 2.

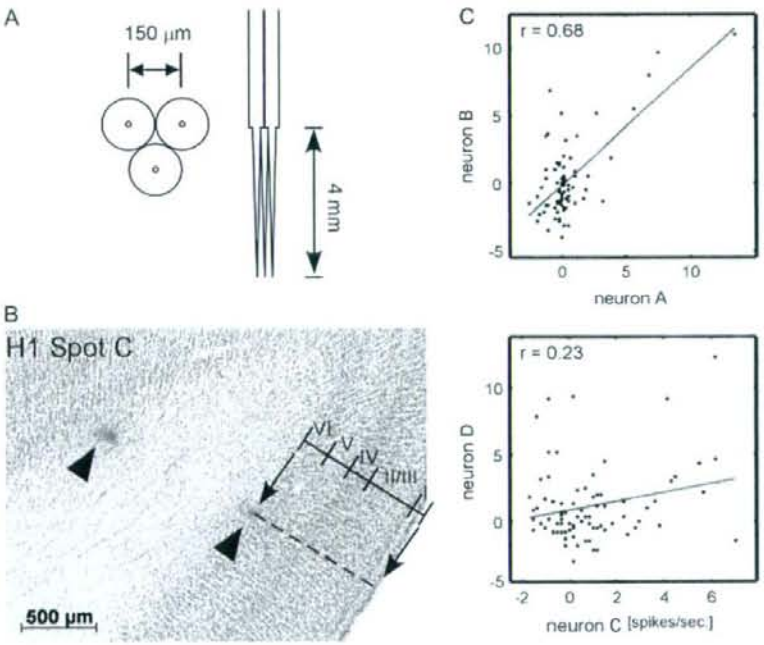

Figure 4. Analysis of the stimulus selectivity of neurons. (*A*) Design of a bundle of tungsten electrodes used in this study. Left and right pictures show the bottom and side view of the electrode bundle. Electrode-to-electrode distance was designed to be about 150 μm at the tip. The exact locations of the electrodes are indicated in Figure 5. (*B*) A histological section of the region including one spot obtained after all the extracellular recording sessions were completed. Two arrowheads indicate the sites of electrocoagulation made at the last penetration of the spot. Based on the depths of the coagulation and borders between the cortical layers, we evaluated the relationship between depth and cortical layers (see Table 1). (*C*) Representative scattergrams indicating similarity in object selectivity of 2 isolated neurons. In each figure, horizontal and vertical axes indicate evoked responses of 2 neurons, and each symbol in the scattergrams indicates an object image. The values of correlation coefficient in the upper and lower panels were 0.68 and 0.23, respectively. These values were statistically significant ($P < 0.05$, number of object images = 80).

fovea. During the stimulus presentation, the stimuli were moved in a circular path (with a radius of 0.4 degree at the rate of 1 cycle/s for intrinsic signal imaging and at 2 cycle/s for extracellular recordings). For intrinsic signal imaging, we used 20 of these stimuli (Fig. 2, top 2 rows) and a gray blank screen for control. For electrophysiological recordings, we recorded responses to all 100 stimuli. Thus, 20 stimuli among these 100 object images were used for both intrinsic signal imaging and extracellular recording sessions.

Intrinsic Signal Imaging

To determine electrode penetration sites for the electrophysiological recording, we investigated spatial patterns of activation induced by visual stimuli using intrinsic signal imaging for 2 monkeys. The exposed cortex was illuminated by light with a wavelength of 605 nm. The reflected light from the cortex was detected by a CCD camera (XC-7500; SONY, Toyko, Japan) through a neutral density filter optimized to the cortex (that made brightness of the cortex spatially homogeneous) and then digitized by a 10-bit video capture board (Pulsar, Matrox, Canada) and stored in a computer (for the neutral density filter, see Przybyszewski et al. 2008). The light was focused to a depth of 500 μm below the cortical surface. The imaged area was 6.4 × 4.8 mm and 320 × 240 pixels. Images of surface blood vessels were made under 540-nm light illumination before intrinsic signal imaging. We presented a visual stimulus to the monkey for 2.0 s. Video signals were acquired for 4.0 s continuously (starting from 1.0 s before the stimulus onset). Twenty stimuli and 2 blank screens were randomly presented, and each of them was repeated 32 times in 1 session. Activity spots, localized regions of activation revealed by intrinsic signal imaging, were extracted as in Tsunoda et al. (2001). The reliability of the intrinsic signal imaging results was examined by conducting the imaging session with the same stimuli on at least 2 different days, and only the activity spots that appeared consistently on these days were investigated (Fig. 3).

Table 1
Estimation of cortical layers from the depth of recording

Cortical layers	Subject	Depth of recording (μm)		
		Upper edge	Lower edge	Thickness
Layer I	H1	82 ± 109	25 ± 107	107 ± 21
	H3	320 ± 478	96 ± 503	194 ± 224
	H2	642 ± 537	404 ± 545	238 ± 10
Layers II and III	H1	25 ± 107	610 ± 144	585 ± 103
	H3	96 ± 503	753 ± 502	841 ± 849
	H2	404 ± 545	454 ± 554	858 ± 124
Layer IV	H1	610 ± 144	822 ± 159	212 ± 42
	H3	753 ± 502	1050 ± 489	259 ± 297
	H2	454 ± 554	729 ± 586	275 ± 45
Layer V	H1	822 ± 159	1072 ± 204	250 ± 46
	H3	1050 ± 489	1382 ± 497	280 ± 331
	H2	729 ± 586	1021 ± 573	292 ± 44
Layer VI	H1	1072 ± 204	1355 ± 222	284 ± 26
	H3	1382 ± 497	1693 ± 536	288 ± 311
	H2	1021 ± 573	1309 ± 591	288 ± 79

Note: The depth was measured from the site where the first extracellular activity was observed at each penetration site. Thus, depth = 0 does not necessarily correspond to the surface of the cortex or the border between layers I and II.

Extracellular Recording

We used bundles of tungsten microelectrodes (FHC, Bowdoin, Maine; catalog# UEWLEJTMNN1E) (Fig. 4A). The shaft of 5 electrodes (diameter, 150 μm) was pasted together with glue to set the electrode-to-electrode distance approximately at 150 μm (Fig. 4A). The bundles of electrodes were inserted into the spots through the artificial dura.

The exposure of the cortex was essential in extracellular recording sessions for 2 reasons. First, in this way, we could visually confirm that the cortical surface was not deformed by electrode penetrations and that the penetration was perpendicular to the cortical surface. Actually, we found that the cortical surface was largely pushed down at the penetration sites with electrode tip angles of 15–20 degree and shank diameter of 120 μm. Thus, in the present study, we used electrodes with a tip angle of 5–7.5 degree and a shank diameter of 70 μm. Lack of deformation was a necessary requirement for precise alignment of depths of recordings and cortical layers as well as for reliable recordings.

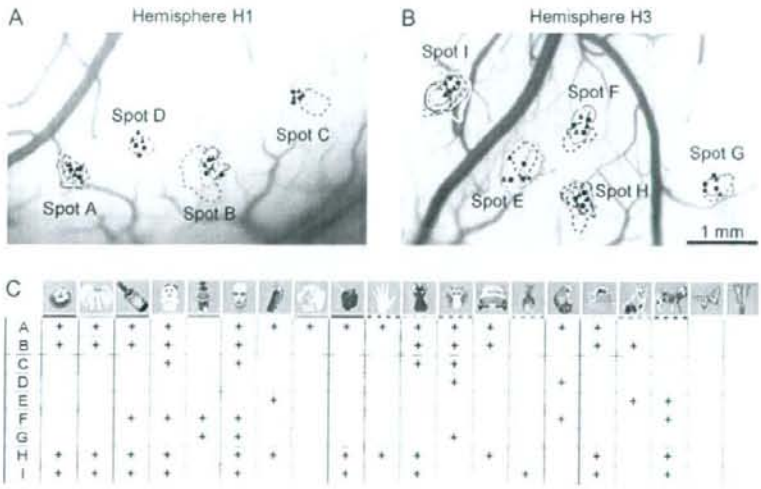

Figure 5. Activity spots revealed by intrinsic signal imaging. (*A*, *B*) Activity spots in H1 (*A*) and H3 (*B*) were demarcated by colored contours. Penetration sites of electrodes are indicated by a filled circle (first-day penetration) and triangle (second-day penetration). (*C*) Optical response patterns of individual spots to 20 stimuli used in intrinsic signal imaging. Each column represents presence (cross) or absence (no symbol) of responses to the stimulus indicated on the top. Rows A–I correspond to spots A–I. The colored horizontal bar under the stimuli is to correlate a stimulus to the activity spots elicited by the stimulus in (*A*) and (*B*). The same color is used for the bar under each stimulus and for the contour of the activity spots elicited by the stimulus. Reliability of intrinsic signal imaging for an individual activity spot was assessed by calculating correlation coefficients between optical responses of the spot and averaged MUAs recorded from the spot for 20 stimuli used for intrinsic signal imaging. The resulting values of the correlation coefficient were 0.85, 0.43, 0.59, and 0.75 for spots A, B, C, and D obtained from H1 and 0.57, 0.50, 0.80, 0.29, and 0.63 for spots E, F, G, H, and I obtained from H3. Because the significant correlation coefficient value was 0.4 for 20 object images ($P < 0.05$), intrinsic signal imaging reliably revealed activity spots except for spot H.

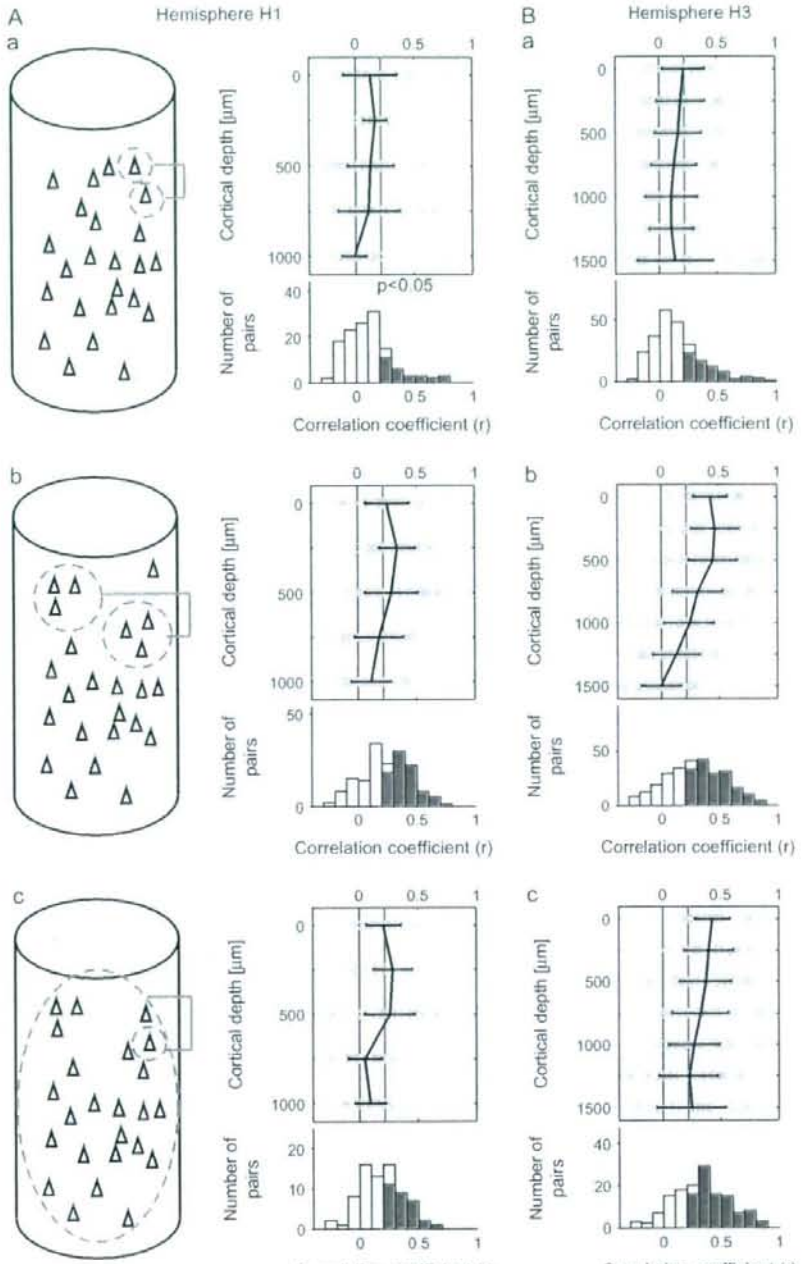

Figure 6. Similarity in stimulus selectivity between single isolated cells (*Aa*, *Ba*), MUs (*Ab*, *Bb*), and between single isolated cells and averaged MUs (*Ac*, *Bc*). (*Aa*, *Ba*) The values of correlation coefficient (*r*) between evoked responses to 80 object stimuli were calculated for isolated single-neuron pairs recorded at the same depth as schematically drawn in (*Aa*) (inset). Upper panels in (*Aa*) and (*Bb*) represent relationships between the *r* values (horizontal axes) and depth of the recording sites of the pairs (vertical axes). The mean (black) and the *r* values of individual pairs (crosses in blue) are indicated. Error bars represent SD. The red vertical line in each panel indicates the statistically significant threshold ($r = 0.22$, $P < 0.05$ for 80 stimuli). Lower histograms in (*Aa*) and (*Ba*) represent the distributions of the pairs with respect to their *r* values. The number of pairs was the sum across the depth. The columns indicated in red represent the number of pairs with significant correlation. The mean value of correlation coefficient (*r*) and the proportion of pairs with significant correlation were 0.11 and 21.2%, respectively, in (*Aa*) and 0.15 and 28.5%, respectively, in (*Ba*). (*Ab*, *Bb*) Correlation between evoked responses to 80 object stimuli were calculated as in (*Aa*) and (*Ba*) for the MU pairs recorded at the same depths as schematically drawn in (*Ab*, inset). Conventions in (*Ab*) and (*Bb*) are the same as (*Aa*) and (*Ba*). In the lower histograms, the mean value of correlation coefficient (*r*) and the proportion of pairs with significant correlation were 0.23 and 51.9%, respectively, in (*Ab*) and 0.28 and 60.0%, respectively, in (*Bb*). (*Ac*, *Bc*) Correlation coefficients were calculated between evoked responses to 80 object stimuli of isolated single neurons and

Second, surface blood vessel patterns were used as landmarks for penetrating electrodes multiple times at the same location.

The electrodes were penetrated perpendicular to the cortex surface. We advanced the electrodes until the first spiking activity was observed. The depth where we found the first spiking activity was set as the baseline depth (0 μm). We recorded neuronal activities for every 250-μm step of electrode advancement. At each depth, we waited for 30 min before recording extracellular activities to make sure that positions of the electrodes were stabilized. In total, 10 recording sessions were conducted for each penetration from depth 0 to 2250 μm. The recordings made below the gray matter were excluded from the analysis.

The raw electrical signals from the electrodes were amplified and band-pass filtered (filter range, 500 Hz–10 kHz). The filtered signals were digitized at 25,000 Hz and stored in a computer. The signals were recorded for 1.5 s in each trial. Visual stimulus presentation started 0.5 s after the onset of a trial and lasted for 0.5 s. The intertrial interval was 50 ms so that a blank period between 2 stimuli was 1050 ms. The different stimuli were presented in pseudorandom order, and 12 trials were made for each stimulus.

Spike Data Analysis

We extracted multiple unit activities (MUAs) and isolated single spikes from the filtered signals of each electrode. To obtain MUAs, we detected time stamps when the filtered signal exceeded a certain threshold. The magnitude of the threshold was set to 3.5 times the standard deviation (SD) of background noise. These time stamps were regarded as spikes of multiple cells (multiple units [MUs]) recorded by the electrode.

Single-cell activities were also isolated from the filtered signals by applying a template matching method to spike waveforms. The isolation was confirmed by interspike interval histograms. We rejected the cell with a particular template if the minimum interspike interval was shorter than the interval corresponding to the refractory period.

The evoked responses for each stimulus of an isolated cell and MU were calculated by subtracting the mean firing rate during the 500-ms period before the stimulus onset from the mean firing rate during the 500-ms period starting from 80 ms after the stimulus onset. The evoked responses were averaged for 12 trials.

In part of the analyses, we generated evoked responses of averaged MUs for each stimulus by averaging evoked responses of all MUs recorded from an activity spot.

Correlation Coefficient as a Measure of Similarity in Object Selectivity

We calculated the value of Pearson correlation coefficient between object responses of a single cell single-cell pair (number of objects = 80). Similarly, we calculated the correlation for MU–MU pairs, averaged MU–single cell pairs, and averaged MU–MU pairs. These values were used as a quantitative measure of similarity in stimulus selectivity of the individual pairs. For single cells and MUs, we used pairs obtained from the same depth regardless of recording days or electrodes. Figure 4(*C*) shows the representative scattergrams of evoked responses of isolated neurons pairs that give correlation values (r) of 0.68 (upper panel) and 0.23 (lower panel).

Histology

To correlate cortical layers and recording depth, we made electrical lesions (5 μA, 20 s) at depths of 1000 and 2250 μm in the second penetration of each spot. After all the recording sessions were completed, we deeply anesthetized the animals, administered a lethal dose of pentobarbital sodium (~70 mg/kg), and perfused transcardially, in sequence, with 0.1 M phosphate-buffered saline (pH 7.4), 1% paraformaldehyde, 10%, 20%, and 30% sucrose. Brains were processed by frozen microtomy at 50-μm thickness. We made Nissl sections of the brain and correlated the depth of recordings and cortical layers (Fig. 4*B* and Table 1).

Results

Intrinsic Signal Imaging to Determine Electrode Penetration Sites

We examined 3 hemispheres (H1, H2, and H3) from 3 monkeys. In hemispheres H1 and H3, we conducted intrinsic signal imaging at the beginning to find candidate sites of columns (activity spots) by using 20 visual stimuli (Fig. 5). At least 2 of these object stimuli (Fig. 5*C*) activated 4 (Fig. 5*A*, spots A–D) and 5 activity spots (Fig. 5*B*, spots E–I) in hemispheres H1 and H3, respectively.

A bundle of 3 electrodes was then penetrated into each spot twice on different days, and thus, we recorded 6 MUAs at each depth of each spot (Fig. 5*A*,*B*). We recorded MUAs at every 250-μm advancement in depth starting from the first MUA at the most superficial layer to the depth of the white matter where no MUA was observed. We examined the relationship between the depth of recording sites and cortical layers after extracellular recording sessions were completed for all the spots (Fig. 4*B* and Table 1). Spacing between electrodes at the surface of the cortex was not as accurate as it was designed to be 150 μm (Fig. 4); nevertheless, the recording sites were well situated within the spots except for spot E (Fig. 5*A*,*B*). Because the results obtained from spot E did not differ from those obtained in the other spots, we put the results from spot E together with other spots.

To examine potential biases introduced by predetermining candidate sites of columns by intrinsic signal imaging, we did not conduct intrinsic signal imaging before extracellular recording sessions in hemisphere H2. Because our method of determining electrode penetration sites was different from that for the other 2 hemispheres, we included a discussion at the end of the results obtained from this hemisphere in comparison with the results obtained from hemispheres H1 and H3.

Similarity of Single-Cell Responses to Object Images

To characterize the response properties of MUs and single cells isolated from MUs, we recorded evoked responses to 100 object images that included 20 object images used for intrinsic signal imaging. We excluded these 20 object images from the main part of the analyses to avoid biasing the results toward stimulus images used for optical imaging. Thus, unless the number of stimuli is explicitly mentioned, the results in the following sections are based on the evoked responses for 80 object stimuli that were not used in the optical imaging sessions. However, as shown below, the results did not largely depend on whether the stimulus responses to the above 20 images were included or not.

We first isolated single-cell activities from MUAs in an off-line analysis. In total, 75 and 143 cells were isolated from MUs recorded from hemispheres H1 and H3, respectively. The similarity in stimulus selectivity of 2 cells recorded at the same depth was then evaluated by calculating the correlation

those of evoked responses of averaged MUs as schematically drawn in (*Ac*) left. Conventions in (*Ac*) and (*Bc*) are the same as (*Aa*) and (*Ba*). In the lower histograms, the mean value of correlation coefficient (r) and the proportion of pairs with significant correlation were 0.18% and 40.0%, respectively, in (*Ac*) and 0.32% and 65.7%, respectively, in (*Bc*). (*A*) are the results obtained from spots A–D (H1), and (*B*) are from spots E–I (H3).

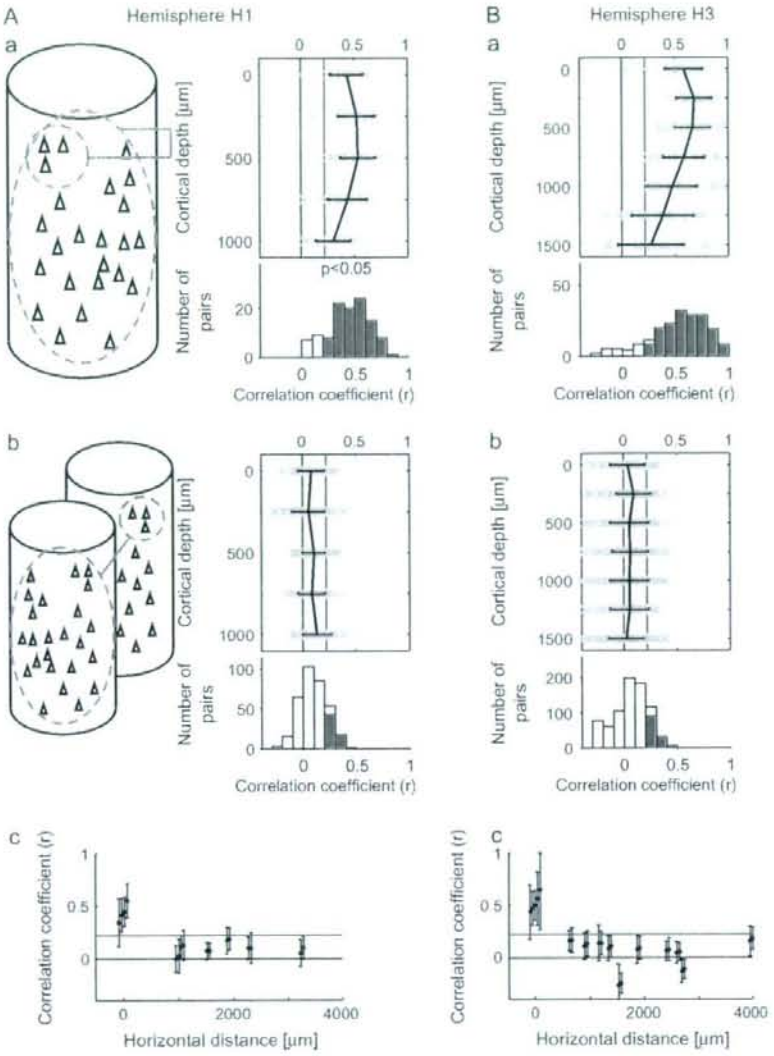

Figure 7. Similarity in stimulus selectivity within a spot and across 2 spots. (*Aa*, *Ba*) The values of correlation coefficient were calculated between evoked responses to 80 object stimuli of averaged MUs and those of evoked responses of individual MUs within the same spots, as schematically drawn in (*Aa*) left. Please note that an MUA was excluded from the averaged MU when correlation coefficient was calculated between this MU and the averaged MU. Conventions in (*Aa*) and (*Ba*) are the same as Figure 6(*Aa*,*Ba*). (*Ab*, *Bb*) Correlation coefficients were calculated between evoked responses to 80 object stimuli of averaged MUs and those of evoked responses of individual MUs in the other spots, as schematically drawn in (*Ab*) left. Conventions in (*Ab*) and (*Bb*) are the same as Figure 6(*Aa*,*Bb*). (*Ac*, *Bc*) The values of the correlation coefficients shown in (*Aa*), (*Ba*), (*Ab*), and (*Bb*) are plotted against distances between spots. To distinguish values obtained from the MUs and averaged MUs of the same spots, the points were slightly displaced from distance 0. The values of correlation coefficients were averaged across the depth. The mean value and SD are plotted. The horizontal red lines indicate statistical significant levels ($P < 0.05$, r 0.22). The distances were measured from the surface images and recording sites (Fig. 5*A*,*B*).

coefficient between evoked responses to 80 stimuli in each of the cell pairs (Figs 4*C* and 6*Aa*). In other words, we quantified the similarity of tuning curves between 2 cells for 80 stimuli by the value of the correlation coefficient. We included the pairs of isolated cells recorded on the different days in our analysis if these cells were recorded at the same depth and from the same spot. Regardless of the depth of recording, mean values of the correlation coefficient (that were below 0.22) indicate that there were no statistically significant correlations ($P > 0.05$) (Fig. 6*Aa*,*Ba*, upper panels). The values of the correlation coefficient for the pairs across all along the depth were only 0.11 ± 0.21 and 0.15 ± 0.22 (mean ± SD) in H1 and H3, respectively (Fig. 6*Aa*,*Ba*, lower panels). Because the evoked response to a stimulus was obtained by averaging for 12 trials, these low correlations could be due to the trial-to-trial variation of the evoked responses. We found, however, that the correlations between the evoked responses obtained by averaging half of the trials (6 trials) of one neuron and

those obtained by averaging of the other half of the trials (6 trials) of the same neuron were 0.37 ± 0.26 and 0.39 ± 0.26 (mean ± SD) for H1 and H3, respectively. These values were significantly higher than the values of correlation coefficient between evoked responses obtained by 6-trial averaging of one cell and those of the other cell (0.10 ± 0.20 and 0.12 ± 0.20 for H1 and H3, respectively; *t*-test, $P < 0.05$). Thus, the low values for correlation coefficient across the cells in respect to stimulus selectivity could not be explained by the trial-to-trial variation of the responses. The proportion of single-cell pairs that had significant values of correlation across depth were only 21.2% (28/132) and 28.5% (70/246) in hemispheres H1 and H3, respectively (Fig. 6*Aa,Ba*, lower panels). The proportions did not significantly change when we included all 100 images (21.2% and 29.7% for H1 and H3, respectively; *t*-test, $P < 0.027$). These results indicate that the observations such as those shown in Figure 1 were not exceptional cases: effective stimuli varied among nearby cells. These results seemingly provide negative evidence for columnar organization in area TE.

Similarity in MU Responses to Object Images

In addition to the extracellular activities of isolated cells, we analyzed MU pairs in the same way: we calculated the value of the correlation coefficient for evoked responses to the stimulus set between 2 MUs recorded from the same depth (Fig. 6*Ab,Bb*). Because activities of identical cells would be detected by adjacent electrodes in the electrode bundle, duplicate detection of spikes in a pair of MUs could cause overestimation of the correlation. To minimize this possibility, we only examined the pairs of MUs recorded on the different days but from the same depth. The values were 0.23 ± 0.20 and 0.28 ± 0.26 (mean ± SD) for H1 and H3, respectively; the mean values were beyond the threshold of statistical significance ($r = 0.22$; *t*-test, $P < 0.05$ with $n = 80$) except those at depths deeper than 750 μm in hemisphere H1 and 1000 μm in hemisphere H3 (Fig. 6*Ab,Bb*, upper panel). The proportions of MU pairs that had significant correlations ($P < 0.05$) calculated across the depth were 51.9% (84/162) and 60.0% (165/275) in hemispheres H1 and H3, respectively (for 100 object images, the proportions were 59.3% and 63.3% for H1 and H3, respectively [$P < 0.027$]) (Fig. 6*Ab,Bb*, lower panels). Because it was unlikely that we recorded from the same cells on different days, a critical factor resulting in higher values of the correlation coefficient compared with single-cell pairs could be that one MUA was the sum of multiple single cellular activities. In one MUA, the summation across the cells would remove the variations of cell-specific responses and extract the common property across single-cell responses (the effect of the averaging further confirmed in Appendix). Accordingly, the high correlation values among MUAs indicate that the common property extracted from one MU was similar to that extracted from the other MUs. This common property was not seen in the analysis of evoked responses of isolated single cells because cell-to-cell variability was too high.

Common Property of Each Spot Extracted by Averaging Activities of MUs

Based on the above interpretation, we characterized response properties of each spot by averaging all the MU responses

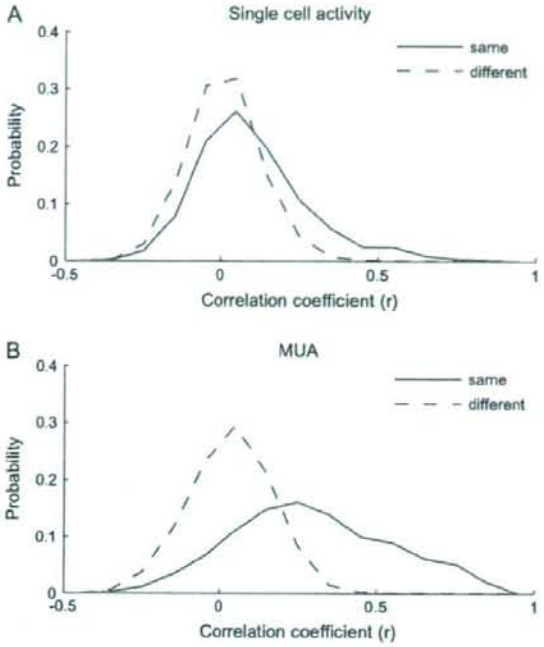

Figure 8. Demonstration that common response properties existed for the cells within an activity spot but did not for cells across the activity spots. (*A*) Distributions of single-neuron pairs with respect to the values of the correlation coefficients between evoked responses to 80 stimuli of the cells in each pair. The solid line represents the distribution of pairs where cells were chosen from the same spots and the dotted line represents the distribution of pairs where cells were chosen from different spots. (*B*) Distributions of MU pairs with respect to the values of the correlation coefficients between evoked responses to 80 stimuli of the MUs in each pair. As in (*A*), the solid line represents the distribution of pairs of MUs from the same spots and the dotted line represents the distribution of pairs of MUs from different spots. Please note that the constituent members of a pair were chosen regardless to the depth that they were recorded from. Thus, in contrast to Figure 6, the members of pairs do not necessarily located close to each other even they are recorded from the same spot.

recorded in the spot. We obtained a set of evoked responses of averaged MUAs by averaging evoked responses of MUs in the same spot for individual stimuli. Then, we calculated the values of the correlation coefficient for evoked responses between averaged MU and those of each isolated single cell obtained from the same spot (Fig. 6*Ac,Bc*). Please note that the MU that included the isolated single cell used for calculating the correlation coefficient was excluded from the averaged MU to avoid overestimation of the value of the correlation coefficient. In comparison with Figure 6(*Aa,Ba*) where evoked responses of 2 single cells were compared, we observed increased correlation up to 500 and 750 μm in cortical depth for hemispheres H1 and H3, respectively (Fig. 6*Ac,Bc*). The proportions of pairs of an averaged MU and a single cell with significant correlations across the depth were as high as 40.0% (30/75) and 65.7% (94/143) in hemispheres H1 and H3, respectively (Fig. 6*Ac,Bc*, lower panels). The values of correlation coefficient were 0.18 ± 0.19 and 0.32 ± 0.24 (mean ± SD) for H1 and H3, respectively. Based on the histological examination, depths of 500 μm in H1 and 750 μm in H3 approximately correspond to the lower edge of layer 4